COMEC

The 10th International Conference on COMPUTATIONAL MECHANICS AND VIRTUAL ENGINEERING

Transilvania University of Brasov
FACULTY OF MECHANICAL ENGINEERING

25-27 October 2023

AEROELASTIC BEHAVIOR OF AN AIRFOIL TYPICAL SECTION CONSIDERING NONLINEAR UNSTEADY AERODYNAMICS

Luís F. M. S. Cassales[1], Lucas V. Caravita[2], Giovanne S. A. Silva[3], Lucas, Vagner C. Sousa[*4]

1. MSc. Candidate – UNESP, São João da Boa Vista, Brazil, luis.cassales@unesp.br
2. MSc. Candidate – UNESP, São João da Boa Vista, Brazil, lucas.caravita@unesp.br
3. Graduating in Aeronautical Engineering - UNESP, São João da Boa Vista, Brazil, giovanne.sooma@unesp.br
4. PhD Assistant Professor - UNESP, São João da Boa Vista, Brazil, vagner.sousa@unesp.br

[*]Corresponding author: vagner.sousa@unesp.br

Abstract: *This study compares simulation results for the aeroelastic behavior of an airfoil typical section by considering two distinct unsteady aerodynamics models: linear and nonlinear, for different airflow speeds. The considered aerodynamic models are the Edwards model, that treats the aerodynamic loading in a linear approximation, and the Beddoes-Leishman model, that treats the aerodynamic loading as a combination of linear and nonlinear contributions. The main goal of this study is to investigate the effects related to the dynamic stall phenomenon at airflow speeds above the linear critical flutter speed. As expected, simulation results show that the Beddoes-Leishman model represents the aeroelastic response of the airfoil more realistic, predicting the transformation of typical flutter unstable responses into stable limit-cycle oscillations at post-flutter airflow speeds.*

Keywords: *Aeroelasticity. Nonlinear aerodynamics. Flutter. Dynamic Stall.*

1. INTRODUCTION

In aeronautical sector, a particularly aeroelastic phenomenon of interest is the flutter, due to its catastrophic potential, being involved in several aeronautical accidents.

Flutter is considered as a dynamic instability, which manifests from a certain flow speed, considered the critical system parameter. Briefly, flutter can be understood as being: stable for speeds below the critical speed, marginally stable at the critical speed and unstable for speeds above the critical speed, where self-sustained oscillations appear. The arise of these self-sustained oscillations is the reason for the catastrophic nature of flutter, since, physically, this denotes into displacements of increasing amplitudes, until the collapse of the structure [1].

For linear aerodynamic models, the typical flutter behavior discussed above is expected. However, under specific conditions, nonlinearities can be

added to the system, so that self-sustaining oscillations of increasing amplitude are replaced by limit-cycle oscillations (LCOs) of constant amplitude [2]. A source of non-linearity are the effects arising from the dynamic stall, which results from the loss of lift forces on the airfoil, due to the separation of the flow [1].

This study aims to compare the response of an aeroelastic system when two different aerodynamic models are used: one of them is the Edwards model, which represents a linear aerodynamics, and the other is the Beddoes-Leishman (BL) model, which represents a non-linear aerodynamics.

2. LITERATURE REVIEW

2.1 Beddoes-Leishman Model

The BL model was initially proposed through the use of indicial functions [3], and later adapted to a state-space representation [4]. The state-space representation was chosen due to its relative ease of implementation.

To represent BL aerodynamics model, there is a system of 12 states ODEs, being: 8 corresponding to the linear portion of the flow, 3 referring to the progressive detachment of the flow at the trailing edge (non-linear phenomenon) and the remaining state corresponds to the dynamic stall process. The states referring to the linear portion are presented in Eq. (2.1.1) and (2.1.2).

$$\{\dot{x}\} = [A]\{x\} + [B]\begin{Bmatrix}\alpha \\ q\end{Bmatrix} \qquad (2.1.1)$$

$$\begin{Bmatrix}C_N^p \\ C_M^p\end{Bmatrix} = [C]\{x\} + [D]\begin{Bmatrix}\alpha \\ q\end{Bmatrix} \qquad (2.1.2)$$

Matrices A, B, C and D are dependent on semi-empirical constants of the model and flow speed [4]. The terms α and q (angle of attack and pitch rate, respectively), are inputs related to the structural part of the problem. Using the response of the linear part of the problem, it is possible to determine the effective angle of attack (α_E), given by Eq. (2.1.3), this term is related to the viscous effects on the airfoil.

$$\alpha_E(t) = \beta^2\left(\frac{2V_\infty}{c}\right)(A_1 x_1 b_1 + A_2 x_2 b_2) \qquad (2.1.3)$$

The first non-linear state is related to the stall. In [5] corrections are proposed taking into account non-stationary conditions for the stall model based on the critical pressure on the leading edge [6]. Thus, the pressure is associated with aerodynamic normal forces (C_N), as well as with a delay due to the non-stationary part (C_N').

$$\dot{x}_9 = \left(\frac{2V_\infty}{c}\right)\frac{-x_9 + C_N^p(t)}{T_P} \qquad (2.1.4)$$

$$x_9 = C_N'(t) \qquad (2.1.5)$$

In Eq. (2.1.4), the term ($2V_\infty/c$) is a constant that makes the equation dimensional, and $C_N^P(t)$ is the value obtained by Eq. (2.1.2) and T_P a constant of time. The value obtained through Eq. (2.1.5) is used to determine the condition of the flow, if $|C_N'| \geq C_{N_1}$ there will be detachment of the flow, where

C_{N_1} is the critical value for the normal force under static conditions, and after the detachment of the flow there will be the reattachment when $|C'_N| < C_{N_1}$.

The next two states are related to aerodynamic loads derived from the Kirchhoff model for a flat plate, and represent flow separation and vortex detachment at the trailing edge of the profile. To find the point where the flow separation occurs, it is necessary to determine an equivalent angle of attack (α_F) [7], which takes into account the non-linear effects and finds an equivalent angle for the static case that would result in the same pressure on the leading edge, thus using the term given by Eq. (2.1.5) and the slope of the normal force curve (C_{N_α}), we have Eq. (2.1.6).

$$\alpha_F = \frac{C'_N}{C_{N_\alpha}} \tag{2.1.6}$$

Using α_F, the position of the flow separation is determined from Eq. (2.1.7). Where the terms s_1 and s_2 are empirical coefficients, and α_1 the static stall angle, considered for a value of $f = 0.7$ in most airfoils. The values adopted were taken from references [8] and [9].

$$f(\alpha) = \begin{cases} 1 - 0.3e^{\frac{|\alpha| - \alpha_1}{s_1}} \; if \; |\alpha| \leq \alpha_1 \\ 0.04 - 0.66e^{\frac{\alpha_1 - |\alpha|}{s_2}} \; if \; |\alpha| > \alpha_1 \end{cases} \tag{2.1.7}$$

$$\dot{x}_{10} = \left(\frac{2V_\infty}{c}\right)\frac{-x_{10} + f(\alpha_F)}{T_f} \tag{2.1.8}$$

$$x_{10} = f''(t) \tag{2.1.9}$$

The term $f''(t)$ corresponds to flow separation due to delays, and T_f varies according to the flow conditions discussed for C'_N. For the vortex detachment condition T_f is given by the conditions presented in Eq. (2.1.10).

$$T_f = \begin{cases} T_{f0} \; if \; 0 \leq \tau_v \leq T_{vl} \; and \; \alpha\dot{\alpha} \geq 0 \\ \frac{1}{3}T_{f0} \; if \; T_{vl} < \tau_v \leq 2T_{vl} \; and \; \alpha\dot{\alpha} \geq 0 \\ \frac{1}{2}T_{f0} \; if \; 0 \leq \tau_v \leq T_{vl} \; and \; \alpha\dot{\alpha} < 0 \\ 4T_{f0} \; if \; 2T_{vl} < \tau_v \end{cases} \tag{2.1.10}$$

T_{f0} and T_{vl} are empirical parameters and $\tau_v = 2V_\infty/c$ a counter that runs with dimensionless time. During this phase, there is a change in α_1, with increments dependent on a $\delta_{\alpha 1}$, according to Eq. (2.1.11).

$$\alpha_1 = \begin{cases} \alpha_{1_0} \; if \; \alpha\dot{\alpha} \geq 0 \\ \alpha_{1_0} - \left(1 - \alpha_{1_0}\right)^{0.25}\delta_{\alpha 1} \; if \; \alpha\dot{\alpha} < 0 \end{cases} \tag{2.1.11}$$

After the flow reattachment, T_f is given by Eq. (2.1.12), and the value of α_1 returns to being the critical angle for the static case.

$$T_f = \begin{cases} T_{f0} \; if \; f'' \geq 0.7 \\ 2T_{f0} \; if \; f'' < 0.7 \end{cases} \tag{2.1.12}$$

$$\alpha_1 = \alpha_{1_0} \tag{2.1.13}$$

The next state comes from a change in the Kirchhoff model for the pitch moment in the vortex shedding region [10]. Where the f_m term of Eq. (2.1.15) is similar to the term described by Eq. (2.1.9).

$$\dot{x}_{11} = \left(\frac{2V_\infty}{c}\right)\frac{2\left(-x_{11} + f(\alpha_F)\right)}{T_{f0}} \qquad (2.1.14)$$

$$x_{11} = f_m(t) \qquad (2.1.15)$$

From the terms obtained previously, the aerodynamic loads can be given by the expressions presented in Eq. (2.1.16).

$$\begin{cases} C_N^f(t) = C_N^c(t)\left(\frac{1+\sqrt{f''}}{2}\right)^2 \\ C_M^f(t) = C_N^c(t)\{K_0 + K_1(1-\hat{f}) + K_2 sin(\pi \hat{f}^2)\} + C_{M_0} \\ C_T^f(t) = \eta C_{N_\alpha}\sqrt{f''}\left(\frac{C_N^c}{C_{N_\alpha}}\right)^2 \end{cases} \qquad (2.1.16)$$

K_0, K_1 and K_2 are empirical values, $\hat{f}$ the greater value between x_{10} and x_{11}, and $C_N^c = C_{N_\alpha}\alpha_E$. The last state refers to dynamic stall. Before the flow detachment, the characteristic vortices are neglected. After the detachment condition is reached the behavior will be given by Eq. (2.1.17) and Eq. (2.1.18).

$$\dot{x}_{12} = \left(\frac{2V_\infty}{c}\right)\frac{-x_{12} + \dot{C}_v}{T_v} \qquad (2.1.17)$$

$$x_{12} = C_N^v(t) \qquad (2.1.18)$$

Empirical terms (T_{v0} and T_{vl}) and the counter τ_v are used for the calculation of the term T_v, described in Eq. (2.1.19).

$$T_v = \begin{cases} T_{v0}\ if\ 0 \le \tau_v \le T_{vl}\ and\ \alpha\dot{\alpha} \ge 0 \\ 0.25T_{v0}\ if\ T_{vl} < \tau_v \le 2T_{vl}\ and\ \alpha\dot{\alpha} \ge 0 \\ 0.5T_{v0}\ if\ 0 \le \tau_v \le T_{vl}\ and\ \alpha\dot{\alpha} < 0 \\ 0.9T_{v0}\ if\ 2T_{vl} < \tau_v \end{cases} \qquad (2.1.19)$$

The normal force coefficient is determined by Eq. (2.1.20) and the moment coefficient by Eq. (2.1.21).

$$C_v = \begin{cases} C_N^c\left[1 - 0.25\left(1+\sqrt{f''}\right)^2\right]\ if\ \tau_v \le 2T_{vl} \\ 0\ if\ \tau_v > 2T_{vl} \end{cases} \qquad (2.1.20)$$

$$C_M^v(t) = -0.25\left[1 - cos\left(\frac{\pi\tau_v}{T_{vl}}\right)\right]C_n^v \qquad (2.1.21)$$

Thus, the final aerodynamic response will be given by Eq. (2.1.22) and (2.1.23).

$$\begin{aligned} C_{m_{ra}}(t) = {} & C_M^p(t) + C_M^f(t) + C_m^v(t) \\ & + \left[C_N^p(t) - C_N^c(t) + C_N^f(t) \right. \\ & \left. + C_N^v(t)\right](X_{ea} - X_{ac}) \end{aligned} \qquad (2.1.22)$$

$$\begin{aligned} C_l(t) = {} & \left[C_N^p(t) - C_N^c(t) + C_N^f(t) + C_N^v(t)\right]cos\alpha(t) \\ & - C_T^f(t)sin\alpha(t) \end{aligned} \qquad (2.1.23)$$

2.2 Structural Model

The structural model uses a typical section with 2-DOF, as described by Fig. 2.2.1. The dimensionless state space representation for the structural part is given in Eq. (2.2.1).

$$\begin{bmatrix} \mu & x_\theta \\ x_\theta & r_\theta^2 \end{bmatrix} \begin{Bmatrix} \ddot{h}(t) \\ \ddot{\theta}(t) \end{Bmatrix} + \begin{bmatrix} \zeta_h & 0 \\ 0 & \zeta_\theta \end{bmatrix} \begin{Bmatrix} \dot{h}(t) \\ \dot{\theta}(t) \end{Bmatrix} + \begin{bmatrix} 1 & 0 \\ 0 & \eta_\theta^2 r_\theta^2 \end{bmatrix} \begin{Bmatrix} h(t) \\ \theta(t) \end{Bmatrix} = \begin{Bmatrix} -\acute{L} \\ \acute{M}_\theta \end{Bmatrix} \tag{2.2.1}$$

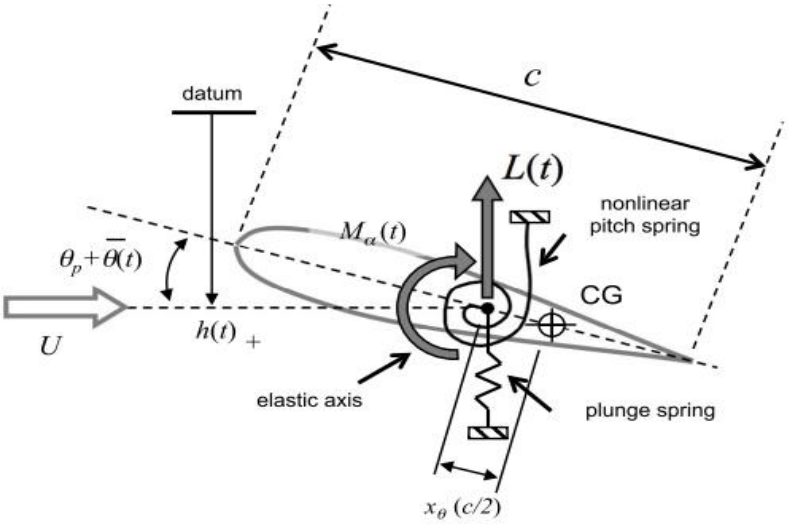

Figure 1: Typical aeroelastic section [9]

Where μ is the ratio of the airfoil mass to the total mass, η_θ is the frequency ratio, r_θ is the dimensionless gyration radius, x_θ is the dimensionless distance between the elastic center and the CG, and ζ_h and ζ_θ are damping ratios [11]. Using the values for the angle of attack (α) and the pitch rate (q), together with Eq. (2.2.2), the inputs for the BL model can be determined.

$$\begin{cases} \alpha(t) = \theta(t) + arctan\left[\dfrac{\dot{h}(t)}{V_\infty}\right] \\ q(t) = \left(\dfrac{c}{V_\infty}\right)\dot{\theta}(t) \end{cases} \tag{2.2.2}$$

3. RESULTS AND DISCUSSION

The results obtained through the Edwards and BL models were compared for speeds greater than and equal to the critical speed (the parameters used were the same as used in [8]). In this case, the V_{cr} found is 14.49 m/s.

Also has been made the comparison between the BL model with the influence of nonlinear parameters and without this influence, the results obtained can be verified through the graphs of θ, h and α, where the first two represent elastic deformations in the airfoil section and the third the angle of attack, determined through the structural equation (2.3.2).

The Fig. 2 shows the results of the models for the critical speed 14.49 m/s, where the amplitudes of the angle of attack, rotation and translation remain constant. The results are very similar between the models, with little

variation in amplitude, so both models still provide reliable results at the critical speed.

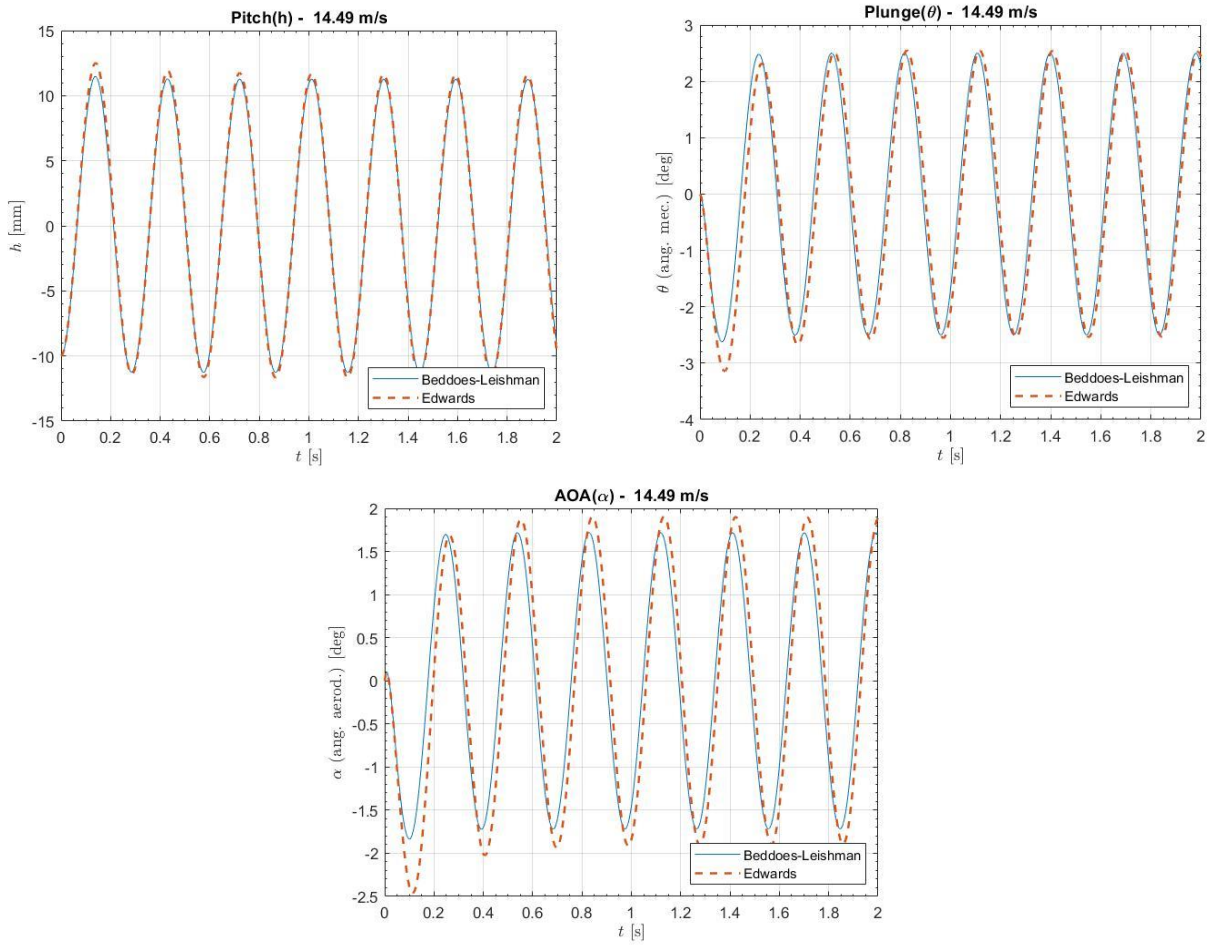

Figure 2: Flutter critical speed [Authors].

At speeds above flutter speed, where a dynamic stall occurs, the difference between the models is noticed. Fig. 3 shows the impact for a speed of 17 m/s, where the BL model reaches a value limit amplitude, which was already expected, due to the effect of the non-linearities generated by the dynamic stall. In the Edwards model, the movements continue to increase in amplitude even after the angle at which the dynamic stall would theoretically occur, since this model does not consider this type of non-linearity.

The differences between the models for high angles of attack is what differentiates them and defines the BL model as much closer to reality in this case. It is also notable that there is a difference in the amplitude of the two models before dynamic stall, where the BL model has larger angles.

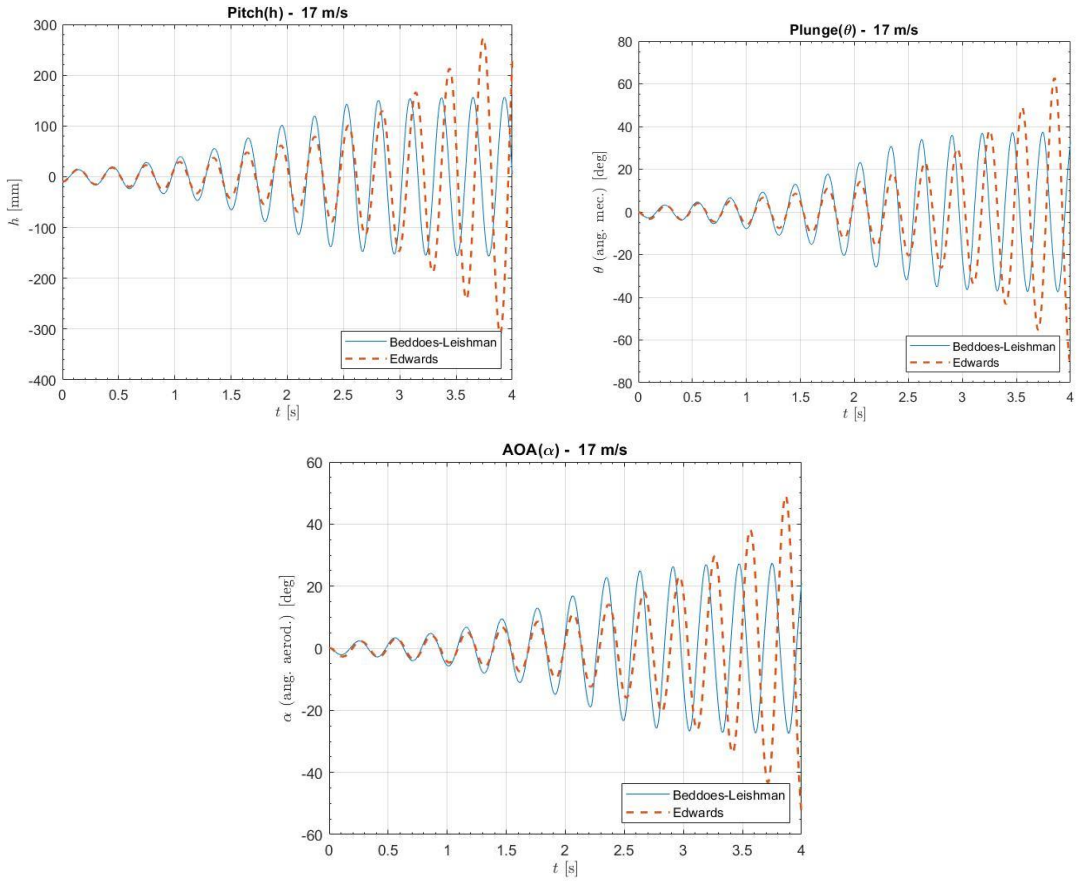

Figure 3: Speeds above the critical speed of flutter [Authors].

When compared, the BL model shows the great difference between considering or not the non-linearities, since from the critical speed there is a very large increase in the amplitude when the effect of the dynamic stall is not considered, making clear the need to consider it when working in this speed range.

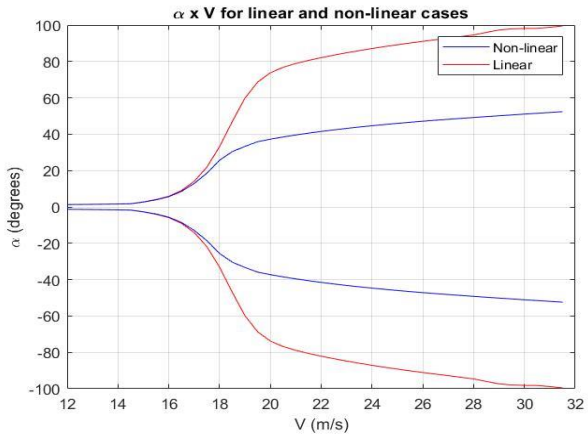

Figure 4: Comparison between linear and non-linear Beddoes-Leishman [Authors].

4. CONCLUSIONS

Two different situations were compared between BL and Edwards methods: the airfoil response for the above cases and the critical flutter speed. The predicted linear flutter speed for the airfoil is 14.49 m/s. At this speed, the

models predict comparable amplitude and frequency. By increasing the speed to 17.0 m/s the amplitude of the models varies. The Edwards model continues to have its amplitude increased continuously while the BL model tends to stabilize at a point.

These results can be explained by the dynamic stall, that decreases the aerodynamic forces at high angles due to detachment of the boundary layer, causing the structural forces to stand out and tend to maintain a maximum and constant range of motion. The results are important to show that the BL model is capable of simulating in a more realistic way the behavior of the airfoil in a case above the flutter speed, being more suitable for simulating events that will occur in this speed range.

BIBLIOGRAFIE

[1] DIMITRIADIS, G.; LI, J. Bifurcation behavior of airfoil undergoing stall flutter oscillations in low-speed wind tunnel. AIAA Journal, AIAA, v. 47, n. 11, p. 2577–2596, 2009.

[2] DOWELL, E. H.; EDWARDS, J.; STRAGNAC, T. W. Nonlinear Aeroelasticity. Journal of Aircraft, AIAA, v. 40, n. 5, p. 857–874, 2003.

[3] LEISHMAN, J. G.; BEDDOES, T. S. A semi-empirical model for dynamic stall. Journal of the American Helicopter Society, v. 34, p. 3–17, 1989.

[4] LEISHMAN, J. G.; CROUSE, G. State-space models for unsteady airfoil behavior and dynamic stall. 30th Structures, Structural Dynamics and Materials Conference, AIAA 89-1319, p. 1372–1383, 1989.

[5] Beddoes, T.S. Onset of Leading Edge Separation Effects Under Dynamic Conditions and Low Mach Number, Proceedings of the 34th Annual Forum of the American Helicopter Society, 1978.

[6] EVANS, W. T.; MORT, K. W. Analysis of computed flow parameters for a set of sudden stalls in low-speed two- dimensional flow. NASA Technical Note, n. D-85, 1959.

[7] CHANTHARASENAWONG, C. Nonlinear Aeroelastic Behaviour of Aerofoils Under Dynamic Stall. PhD Thesis - University of London, South Kensington, London - UK, 2007.

[8] SANTOS, C. R. dos; PEREIRA, D. A.; MARQUES, F. D. On limit cycle oscillations of typical aeroelastic section with different preset angles of incidence at low airspeeds. Journal of Fluids and Structures, ELSEVIER, v. 74, p. 19–34, 2017.

[9] SANTOS, C. R. dos; MARQUES, F. D.; HAJJ, M. R. The effects of structural and aerodynamic nonlinearities on the energy harvesting from airfoil stall-induced oscillations. Journal of Vibration and Control, SAGE, v. 25, n. 14, p. 1991–2007, 2019.

[10] LEISHMAN, J. G.; BEDDOES, T. S. A generalized model for airfoil unsteady aerodynamic behavior and dynamic stall using indicial method. 42nd Annual Forum of the American Helicopter Society, 1986.

[11] SOUSA, V. C.; MARQUI, C. J. de. Effect of pseudoelastic hysteresis of shape memory alloy springs on the aeroelastic behavior of a typical airfoil section. Journal of Intelligent Material Systems and Structures, SAGE, v. 27, n. 1, p. 117–133, 2014.